

Electronic Supplementary Material

for

Climate simulations for 1880-2003 with GISS modelE

by J. Hansen et al.

S1. Alternative Data Samplings and the Krakatau Problem

Comparisons of simulated climate and observations commonly involve choices that influence how well the model and data appear to agree. Choices of surface temperature data deserve scrutiny, because surface temperature provides the usual measure of long-term ‘global warming’ as well as a test of possible global cooling after large volcanic eruptions. We illustrate here alternative comparisons of model and observations, with model results being those of the coupled model (ocean C, the *Russell et al.* [1995] model) driven by all climate forcings of Fig. 5. This model run is discussed in later sections.

S1.1. Century time-scale

Temperature measurements at meteorological stations provide a reasonably consistent data set for continental and island locations (*Jones et al.* 1986; *Hansen and Lebedeff* 1987), albeit one in which the station records are spatially inhomogeneous, often broken temporally, and subject to non-climatic effects. The meteorological station records that we employ have been adjusted for urban effects using neighboring rural stations (*Hansen et al.* 2001). Such adjustments are imperfect, but the impact on global mean 100-year temperature change of uncertainties in urban adjustments is not larger than about 0.1°C (*IPCC* 2001). For the short interval after a volcano considered here, urban adjustments are negligible.

The GISS analysis of station data (*Hansen et al.* 1981; *Hansen and Lebedeff* 1987) combines stations with overlapping periods of record so as to preserve information on temporal variability while allowing individual stations to affect estimated temperature change at distances up to 1200 km. It has been shown, by sampling a global model with realistic temperature variability at the station locations, that after about 1880 the station network is capable of yielding a good estimate of global temperature change despite poor coverage in the Southern Hemisphere (*Hansen and Lebedeff* 1987). However, island and coastal stations fail to sample part of the ocean, and both observations and models indicate that the long-term temperature response tends to be less over the ocean than over continental areas. Thus we expect the long-term “global” temperature change estimated from the meteorological station network alone to slightly overestimate true global mean temperature change.

Improved global coverage is obtained by combining meteorological station data with sea surface temperature (SST) measurements of ocean areas (*Jones et al.* 1999; *Hansen et al.* 2001). However, ocean data have their own problems, including changes of measurement methods and infrequent sampling of large regions (*Parker et al.* 1994). Sampling is especially poor in the 1800s, and spatial-temporal data-fill procedures risk smoothing real variations. In addition, the ocean area with the largest response to climate forcings in climate models, regions of sea ice, are practically unobserved.

Fig. S1a shows an estimate of global temperature using only meteorological station measurements (*Hansen et al.* 2001). The observed 1880-2003 temperature change, based on the lin-

ear trend, is 0.69°C in this case. The model 5-run “all forcings” ensemble mean yields 0.56°C, with the model result being a true global mean.

Fig. S1b uses the same land temperatures as in Fig. S1a, but it adds SST data for the oceans, using ship data of *Rayner et al.* (2003) for 1880-1981 and subsequently satellite data (*Reynolds and Smith* 1994; *Smith and Reynolds* 2004). Inclusion of ocean data reduces the observed global temperature change to 0.59°C. It also practically eliminates evidence for cooling after the 1883 Krakatau eruption.

Fig. S1c is a third alternative, comparing observed temperature from meteorological stations with the model sampled at the places and times of the observations. This sampled model data is run through the same temperature analysis program as observations to produce the global mean. This third procedure is optimum in the sense of having the most consistent treatment of model and data, as well as preserving a best estimate for high frequency temperature change in the period of sparse observations in the 1800s. The model sampled at observing stations yields a global warming of 0.59°C based on the linear trend, which is less than the observed 0.69°C. This discrepancy occurs because the model warms less over land areas than observed, a result that we identify with excessive anthropogenic tropospheric aerosols over Eurasia in our standard “all forcings”, as discussed in Sect. 5. This third procedure provides a clean comparison of model and observations, but the integration over the globe is not a true global mean. In addition, it is unlikely that most modelers will sample their model results at the times and places of meteorological station measurements and run the results through the GISS temperature analysis program, thus making it difficult to compare GISS model results with other models.

Fig. S1d is a fourth alternative, comparing model results for the true global mean with observations that use only meteorological stations for 1880-1900 but add ocean data for 1900-2003, when ship data had better coverage. This alternative preserves temperature variations in the 1800s without exaggerating long-term global temperature change. The observed 1880-2003 temperature change in this case, 0.61°C, is slightly larger than in Fig. S1b, as expected due to the cooling in the 1880s. The disadvantage of this fourth alternative is the arbitrariness inherent in concatenating two data sets.

We present all four alternatives to help readers make their own assessment. For simplicity we use the procedure of Fig. S1b in following sections, i.e., we use the true global mean for the model and the land + ocean data for observations. However, it should be born in mind that these observations probably miss some actual cooling after Krakatau.

We examine the Krakatau period in more detail, because it has an effect on how well the model and observations appear to agree over the 120-year temperature record. We find it useful to compare the 1883 Krakatau and 1991 Pinatubo eruptions, the two largest volcanic aerosol climate forcings in the period of instrumental climate data (*Sato et al.* 1993). These volcanoes have the best chance of producing signals above the climate noise level and the Pinatubo period has extensive climate observations.

S1.2. Temperature change after Krakatau and Pinatubo

Estimated aerosol optical depths after Krakatau and Pinatubo are shown in Fig. S2a. The shape of the Krakatau curve is assumed to be similar to that after Pinatubo, as they were both low latitude injections to high altitudes at similar times of year. Measurements of decreased solar irradiance integrated over

three years after Krakatau were used to set the aerosol optical depth (Sato *et al.* 1993). Effective forcings are shown in Fig. S2b. Resulting temperature anomalies, relative to the three-year mean preceding the eruption, are shown in Fig. S2c. The simulated cooling after Krakatau exceeds that after Pinatubo by more than the assumed 10% difference in their forcings. This must be at least in part because of planetary radiation imbalance of about $+0.5 \text{ W/m}^2$ that existed just prior to the Pinatubo eruption (Hansen *et al.* 1993) but not at the time of the Krakatau eruption. Further, as mentioned in Sect. 3.2.1, the response to the Krakatau aerosols would have been reduced about 10 percent if the control run ocean temperatures had included the effect of prior volcanic eruptions via a mean stratospheric aerosol optical depth.

Fig. S2c shows that the global mean temperature based on meteorological station data after Krakatau is consistent with the climate simulations. The seasonal mean 1σ error bar for global temperature estimated from the meteorological station network in the 1880s is 0.15°C (Hansen and Lebedeff 1987). Thus the cooling observed by the station network after Krakatau for a given season could be a sampling error, but not the nearly continuous cool period for several years after the eruption. Furthermore, comparison of the global temperature curve estimated from meteorological stations in the Pinatubo era (right side of Fig. S2c) with the global temperature curve that has complete ocean coverage from satellite data shows that the station network tracks the complete global data within the expected error for the station network (1σ sampling error being 0.09°C for the station distribution in the 1990s). We conclude that there was global cooling after Krakatau.

Fig. S2d shows the observed and simulated surface temperature anomalies in the northern winter (DJF) following the eruptions and the northern summer (JJA) about one year after the eruptions. As expected, the model and observations show strong cooling in the summer after the eruption, especially over the continents. Also, the model and observations show global cooling in DJF, with evidence for regional Eurasian “winter warming”, an expected dynamical response (Groisman 1992; Perlwitz and Graf 1995; Robock 2000; Shindell *et al.* 2001), which has previously been reported to occur in current GISS models (Shindell *et al.* 2004). The model, using the coarse-resolution Russell *et al.* (1995) ocean, is not able to produce El Ninos, which have accompanied several large volcanoes in the past century (Handler 1984; Robock 2000; Mann *et al.* 2005) and may be responsible for warming in the region of Alaska. Temperature anomalies are muted in the 5-run model mean in Fig. S2d, but the magnitude of anomalies is more realistic in the individual runs, which are available on the GISS web-site.

S2. Mean Stratospheric Aerosols in Control Run

Our control run had no stratospheric aerosols. Aerosols from the 1883 Krakatau eruption caused ocean heat content in the experiment runs to fall below that in the control run, as expected. However, despite steadily increasing greenhouse gases, the ocean heat content did not recover to that of the control run until about 2000. In reality, ocean temperature is also influenced by volcanoes that erupted prior to 1880. Ideally, ocean initial conditions in 1880 would be obtained from a spin-up run that had time-dependent forcings, including volcanoes, for several centuries prior to 1880. That is not usually practical, if for no other reason than the absence of information on earlier volcanic eruptions. However, it is easy to include a mean stratospheric

aerosol amount in the control run.

Current control runs with our model include a mean stratospheric aerosol optical thickness $\tau = 0.0125$ at $0.55 \mu\text{m}$ wavelength, which is the 1850-2000 mean value of the Sato *et al.* (1993) aerosol climatology. The equilibrium global (surface) cooling for $\tau = 0.0125$ (10% of the maximum τ for Pinatubo) is $\sim -0.2^\circ\text{C}$, and the effect on deeper ocean temperatures is sufficient to alter the rate of ocean heat storage in transient climate simulations. Using a control run in which the ocean temperature had equilibrated with an atmosphere including this mean aerosol amount, we carried out an ensemble of runs for 1850-2003. The concentration of volcanoes near the end of the 19th century caused the ocean heat content anomaly to be negative for several decades, but it recovered to the control run value by the mid 20th century and it subsequently increased at a rate comparable to that reported by Levitus *et al.* (2000).

S3. Control Run Disequilibrium and Drift.

Our coupled atmosphere-ocean (ocean C) simulations, to meet the deadline for submission to IPCC, were initiated before the control run (which provides initial conditions for the experiments) had reached equilibrium, i.e., while there was still an imbalance between the amounts of energy absorbed and emitted by the planet. As a result, the model response to any forcing included a small drift.

We minimize drift effects by subtracting, year-by-year, the same quantities from the same period of the control run. This procedure yields diagnostics with ‘double noise’, i.e., it contains unforced variability of both the control and experiment runs, while the real world has only a single source of unforced variability. Double noise can be minimized by initiating additional control runs at the same points at which experiments are initiated.

An alternative way to remove drift is to calculate and subtract from the experiment result the mean drift in the control over the period of the experiment. For example, for a 124-year 1880-2003 experiment initiated at year X of the control run, we could calculate the linear trends of control run diagnostics over the period X to X + 123 and subtract the control run diagnostics based on their linear trends from the corresponding quantities in the experiment run. This alternative procedure avoids year-to-year double noise, but it does not eliminate drift effects entirely because variability occurs on all time scales.

Noise effects were exacerbated by the fact that most of our experiments, with individual forcings and with multiple forcings, were initiated at the same points of the control run. The control run has unforced variability not only interannually, but on 124-year and all other time scales. Thus when we add up responses to individual forcings, with drift subtracted, we are including the same unforced 124 year fluctuation for each forcing. Therefore we cannot expect the sum of the responses to individual forcings to equal the response to the sum of the forcings, even if there is no non-linearity in the climate response.

An improved procedure would be to initiate experiments for different forcings at different points on the control run, in addition to spacing ensemble members. It would perhaps be still better to carry out a long control run that reaches equilibrium before experiments are initiated, so there would be no need to subtract a control run. However, the merits of waiting until the control run equilibrates before initiating experiments may be reduced if the equilibrium climate drifts too far from the real world.

S4. Surface Temperature Definition.

Surface air temperature (Ts) in modelE is calculated at 10 m height. The land-ocean temperature index (Tx) (Hansen *et al.* 2001) is from observations at 2 m height at meteorological stations and SST data of Rayner *et al.* (2003) and Reynolds and Smith (1994) over the ocean. Temperature changes of model and observations are compared, which minimizes, but does not eliminate, the effect of these height differences.

Fig. S3 shows the modeled 1880-2003 temperature change for (1) ocean A driven by no forcings except SST and sea ice change, (2) the same as (1) but including “all forcings” (GHGs, aerosols, etc.), (3) the same as (2), but for the coupled atmosphere-ocean climate model. For each of these three models we show the global surface air temperature (Ts), the temperature index (Tx), which uses the ocean temperature instead of Ts for ocean areas, and their difference.

In the case of ocean A with no forcings, Ts and Tx are practically the same on global average, even though there are regions where they differ by a few tenths of a degree. In the case of ocean A with radiative forcings, the forcings are able to change atmospheric temperature slightly even though SST is fixed. Global mean Ts increases 0.03°C more than Tx increases over the period 1880-2003. In the case of ocean C the ocean temperature is able to respond to the change of near surface temperature gradient, and Ts increases 0.05°C more than Tx increases over the 1880-2003 period.

These comparisons indicate that our use of global Ts at 10 m height overstates global mean ΔT by several hundredths of a degree, if our aim is comparison with a temperature index that uses SSTs. We could employ ΔTx from the model based on the first layer ocean temperature, but that would be inconsistent with the procedure used in previous studies with the GISS model and other models, and thus we used ΔTs in this paper. This issue may be noticeable only in the GISS model, which calculates Ts in an iterative fashion (Hansen *et al.* 1983; *modelE* 2006). In the future the issue might be practically eliminated by calculating Ts at 2 m height, rather than 10 m.

These small changes in ΔT do not alter the geographical pattern of the discrepancy between model and observations. The main implication is that the 124-year warming in our model with “all forcings” is $\sim 0.10^\circ\text{C}$ less than observed, rather than 0.05°C less. Thus the need for less tropospheric aerosol amount becomes clearer in the global mean temperature, as well as from unrealistic cooling over Europe.

As future models are better able to simulate observed climate change, it will be worth removing any such discrepancy in comparison with observed surface temperature. We are uncertain whether this comparison issue exists for other climate models.

S5. Ozone Scenario.

The first set of runs that we provided to IPCC inadvertently used the Randel and Wu (1999) decadal rate of stratospheric O₃ depletion as the 18-year change, thus understating stratospheric O₃ depletion by the factor 10/18. Corrected runs were submitted several months later, and both sets of runs remain available at www-pcmdi.llnl.gov/ipcc/about_ipcc.php. The correction reduced the 1880-2003 global forcing Fa by 0.03 W/m². The main impact of the correction was on stratospheric cooling in the Antarctic region during the time of O₃ depletion, with the corrected results providing better agreement with observations. The present paper and Efficacy (2005) use the corrected O₃ change.

A second issue with the O₃ scenario concerns O₃ forcing due to tropospheric pollution. The O₃ scenario was derived from an off-line simulation of a tropospheric chemistry model (Shindell *et al.* 2003), which yielded an 1880-2000 O₃ change from the surface to the 150 hPa level at all latitudes. Global forcings for this O₃ change were $F_i = 0.44$, $F_a = 0.38$ W/m². However, tropospheric O₃ forcing implemented in our transient simulations was less, as high-latitude O₃ increases above the model’s tropopause (Fig. 3 of Efficacy [2005]) were excluded, reducing O₃ forcing by 0.05 W/m². As the pollution effect on O₃ at low latitudes was only allowed to reach the 150 hPa level, we suspect that our total O₃ forcing ($F_a = 0.28$, $F_s = 0.26$, $F_e = 0.23$ W/m², including tropospheric pollution and stratospheric depletion, from Table 1) underestimates actual O₃ forcing. Future O₃ scenarios should be generated by models with improved vertical resolution and higher model top, preferably integrating effects of tropospheric pollution and stratospheric change.

S6. Snow Albedo.

A computer programming error was present in the calculation of snow albedo in several of our climate simulations. Some of these runs were repeated with the error corrected, as delineated below. Our intention was for snow albedo change to be proportional to BC deposition as calculated by the aerosol transport model of Koch (2001). The error caused albedo change to be exaggerated in partially snow-covered land gridboxes and understated over sea ice, because total albedo change was fixed.

Our initial ‘all forcing’ run provided to IPCC contained both the ozone error (A.4) and snow albedo error (A.5). We also provided to IPCC ‘all forcing’ runs with the ozone error corrected and later runs with both errors corrected. Because of space limitations, the DOE web site includes only the original ‘all forcing’ ensemble and the ensemble with the ozone forcing corrected. All three ensembles are available on the GISS web site.

The ‘all forcing’ and snow albedo alone ensembles were rerun with the snow albedo error corrected. The corrected program was also used in ‘Arctic pollution’ runs (Fig. 5 in Dangerous [2006]). However, the AltAer1, AltAer3, and AltSol runs contain the snow albedo error, but not the ozone error. These ensembles were not rerun with corrected snow albedo because of the small magnitude of the error and the fact that it would not alter conclusions from those runs. To allow precise comparison with AltAer1, AltAer2, and AltSol, the standard model results in Fig. 16 of this paper and Fig. 6 in Dangerous (2006) are the ‘all forcing’ results that include the snow albedo error.

The simulations employed in the energy imbalance study of Hansen *et al.* (2005b) contained both errors. The errors in global forcing, $+0.03$ W/m² and -0.02 W/m², opposed each other, but regional and temporal effects would not cancel, e.g., stratospheric cooling over Antarctica was underestimated. However, the magnitude of these errors is too small to affect conclusions of that paper.

Efficacy (2005) simulations included the snow albedo error but not the ozone error. In Table 4 and Fig. 16 of Efficacy (2005) the snow albedo forcing was calculated with the incorrect program. F_a was actually 0.05 W/m², not 0.08 W/m², and the correct efficacy for the snow albedo effect was $E_a \sim 2.7$, not $E_a \sim 1.7$.

References to Supplementary Material

Groisman PY (1992) Possible climate consequences of the Pinatubo eruption: An empirical approach. *Geophys Res Lett* 19:1603–1606.
 Handler P (1984) Possible association of stratospheric aerosols and El Niño type events. *Geophys Res Lett* 11:1121–1124.

- Hansen J, Johnson D, Lacis A, Lebedeff S, Lee P, Rind D, Russell G (1981) Climate impact of increasing atmospheric carbon dioxide. *Science* 213:957–966.
- Hansen J, Russell G, Rind D, Stone P, Lacis A, Lebedeff S, Ruedy R, Travis L (1983) Efficient three-dimensional global models for climate studies: Models I and II. *Mon Weather Rev* 111:609–662.
- Hansen J, Lebedeff S (1987) Global trends of measured surface air temperature. *J Geophys Res* 92:13345–13372.
- Hansen J, Lacis A, Ruedy R, Sato M, Wilson H (1993) How sensitive is the world's climate? *Natl Geogr Res Explor* 9:142–158.
- Hansen J, Ruedy R, Glascoe J, Sato M (1999) GISS analysis of surface temperature change. *J Geophys Res* 104:30997-31022.
- Hansen J, Ruedy R, Sato M, Imhoff M, Lawrence W, Easterling D, Peterson T, Karl T (2001) A closer look at United States and global surface temperature change. *J Geophys Res* 106:23947–23963.
- Hansen J et al (2005a) Efficacy of climate forcings. *J Geophys Res* 110: D18104. DOI 10.1029/2005JD005776.
- Hansen J et al (2005b) Earth's energy imbalance: confirmation and implications. *Science* 308:1431–1435.
- Hansen J et al (2006b) Dangerous human-made interference with climate: A GISS modelE study. *Atmos Chem Phys Discuss* 6:12549–12610.
- Intergovernmental Panel on Climate Change (IPCC) (2001) *Climate Change 2001: The Scientific Basis*. Houghton JT, Ding Y, Griggs DJ, Noguer M, van der Linden PJ, Dai X, Maskell K, Johnson CA (eds) Cambridge University Press, Cambridge, UK.
- Jones PD, Wigley TML, Wright PB (1986) Global temperature variations between 1861 and 1984. *Nature* 322:430–434.
- Jones PD, New M, Parker DF, Martin S, Rigor LG (1999) Surface air temperature and its changes over the past 150 years. *Rev Geophys* 37:173–199.
- Koch D (2001) Transport and direct radiative forcing of carbonaceous and sulfate aerosols in the GISS GCM. *J Geophys Res* 106:20311–20332.
- Levitus S, Antonov J, Boyer TP, Stephens C (2000) Warming of the world ocean. *Science* 287:2225–2229.
- Mann ME, Cane MA, Zebiak SE, Clement A (2005) Volcanic and solar forcing of the tropical Pacific over the past 1000 years. *J Clim* 18:447–456.
- Parker DE, Jones PD, Folland CK, Bevan A (1994) Interdecadal changes of surface temperature since the late nineteenth century. *J Geophys Res* 99:14373–14399.
- Perlwitz J, Graf HF (1995) The statistical connection between tropospheric and stratospheric circulation of the Northern Hemisphere in winter. *J Clim* 8:2281–2295.
- Randel WJ, Wu F (1999) A stratospheric ozone trends data set for global modeling studies. *Geophys Res Lett* 26:3089–3092.
- Rayner NA, Parker DE, Horton EB, Folland CK, Alexander LV, Rowell DP, Kent EC, Kaplan A (2003) Global analyses of SST, sea ice and night marine air temperatures since the late nineteenth century. *J Geophys Res* 108(D14):4407. DOI 10.1029/2002JD002670.
- Reynolds RW, Smith TM (1994) Improved global sea surface temperature analyses. *J Clim* 7:929–948.
- Robock A (2000) Volcanic eruptions and climate. *Rev Geophys* 38:191–219.
- Russell GL, Miller JR, Rind DH (1995) A coupled atmosphere-ocean model for transient climate change. *Atmos Ocean* 33:683–730.
- Sato M, Hansen J, McCormick MP, Pollack JP (1993) Stratospheric aerosol optical depths, 1850-1990. *J Geophys Res* 98:22987–22994.
- Schmidt GA et al (2006) Present day atmospheric simulations using GISS ModelE: Comparison to in-situ, satellite and reanalysis data. *J Clim* 19:153–192.
- Shindell D, Schmidt GA, Miller RL, Rind D (2001) Northern Hemisphere winter climate response to greenhouse gas, volcanic, ozone and solar forcing. *J Geophys Res* 106:7193–7210.
- Shindell DT, Fulavegi G, Bell N (2003) Preindustrial-to-present-day radiative forcing by tropospheric ozone from improved simulations with the GISS chemistry-climate GCM. *Atmos Chem Phys* 3:1675–1702.
- Shindell DT, Schmidt GA, Mann ME, Fulavegi G (2004) Dynamic winter climate response to large tropical volcanic eruptions since 1600. *J Geophys Res* 109:D05104. DOI 10.1029/2003JD004151.
- Smith TM, Reynolds RW (2004) Improved extended reconstruction of SST (1854-1997). *J Clim* 17:2466–2477.

Supplementary Figures

Fig. S1. Observed and modeled global surface temperature change for alternative ways of averaging over the globe, with the model driven by all forcings of Fig. 5. (a) Observations are surface air temperature at meteorological stations averaged as defined by *Hansen et al.* (1999), model is true global mean. (b) Observed temperatures are surface air measurements at meteorological stations combined with SST measurements over the ocean, model is true global mean. (c) Observations are at meteorological stations as in Fig. S1a, model is sampled at the same places and times and analyzed in the same way as observations. (d) Model is true global mean, observations are based only on meteorological stations during 1880-1900, but incorporate SSTs after 1900.

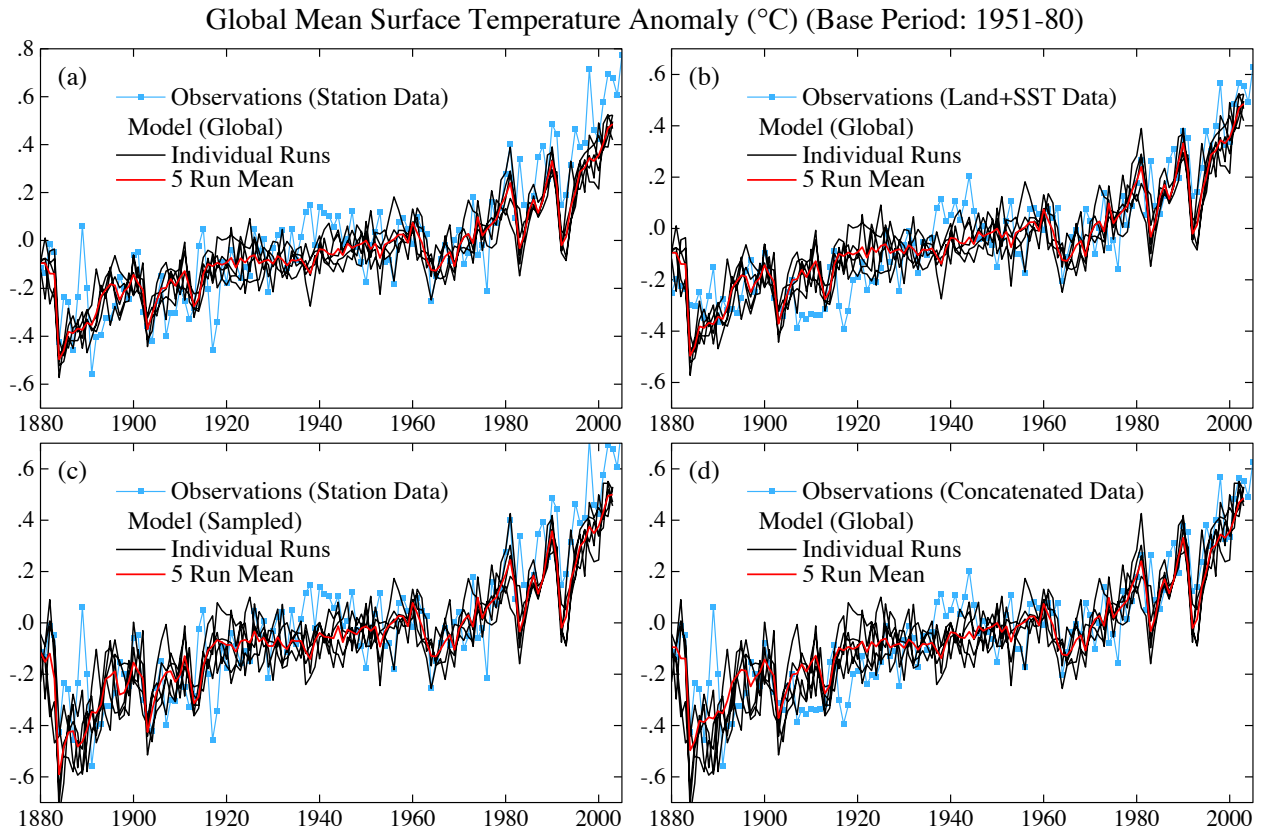


Fig. S2. (a) Stratospheric aerosol optical thickness and (b) effective forcing for the assumed aerosol scenario, based on update of *Sato et al.* (1993). (c, d) Temperatures simulated by the climate model normalized to the mean for the 36 months before the eruption, with the circles and asterisks in (c) being the Jun-Jul-Aug and Dec-Jan-Feb means, respectively. Observed ‘station’ data and ‘land + ocean’ are based on analyses of *Hansen et al.* (2001), using, respectively, meteorological stations alone and those same stations plus ocean data of *Rayner et al.* (2003).

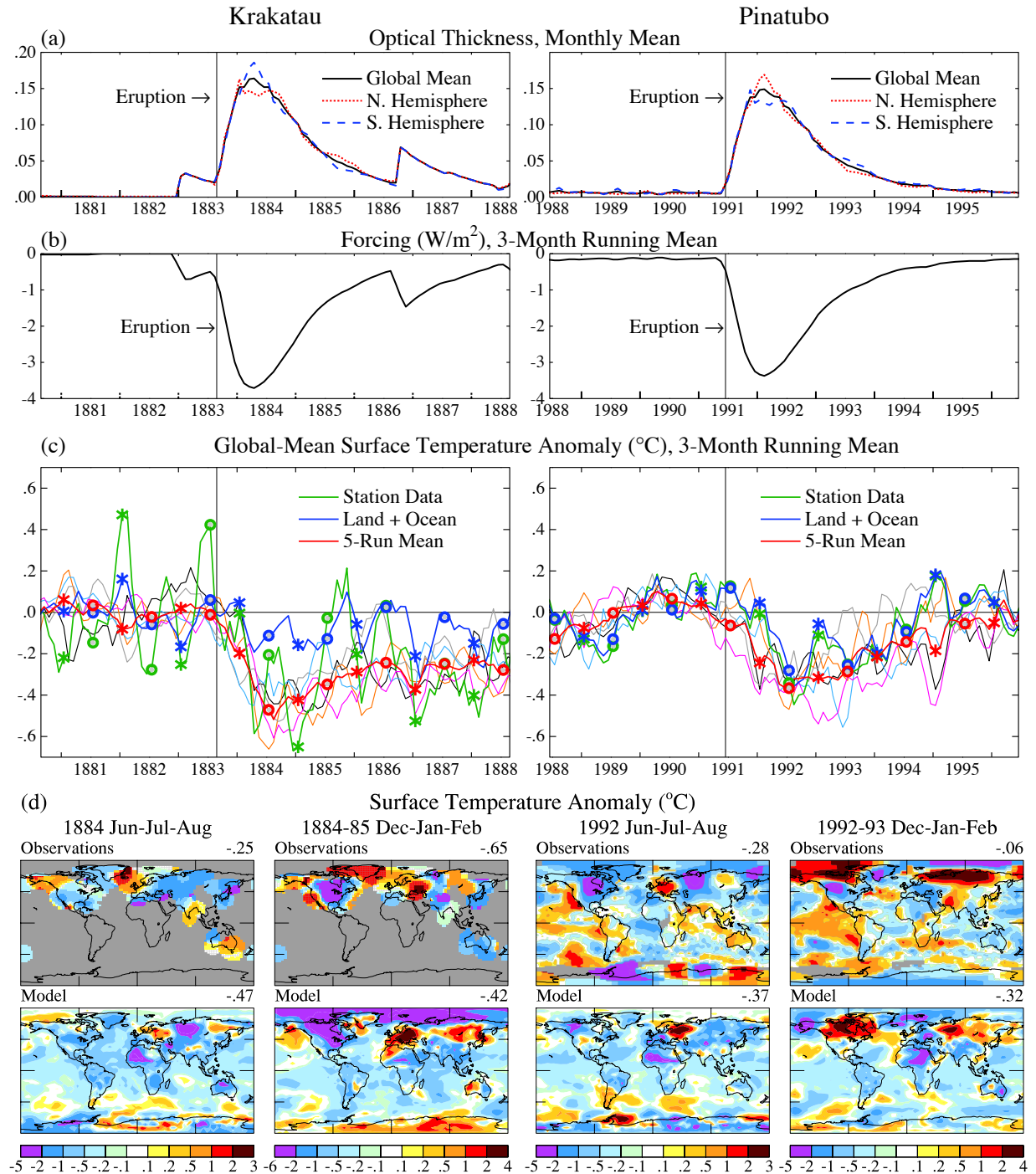


Fig. S3. Simulated surface temperature change for 1880-2003 based on local linear trends. Ts is the surface air temperature at 10 m altitude, Tx substitutes SST for Ts over the ocean. Ocean A uses the SST and sea ice history of *Rayner et al.* (2003) coupled to atmospheric modelE, while ocean C couples modelE with the *Russell et al.* (1995) ocean model.

